CHAPTER 4
MEASUREMENT OF PRECIPITABLE WATER WITH THE MICROWAVE WATER VAPOUR RADIOMETER

4.1 Introduction

It is well known that the atmospheric noise level at microwave and millimeter wave frequencies is determined by the absorption and radiation of atmospheric gases and associated condensation and precipitation products. The relationship between microwave thermal emission and atmospheric moisture was first observed by Dicke et al (1946). The possibility of measuring the concentration of atmospheric constituents from multispectral emission or extinction observations in the microwave region was discussed by Barret and Chung (1962) and Staelin (1966) and demonstrated by Staelin (1969) and Toong and Staelin (1970), who obtained values of water vapour concentration and liquid water content of clouds from emission observations at five frequencies.

The earliest passive microwave observations were made in 1945 by Dicke (1946) at 1.00, 1.25 and 1.50 cm wavelengths. Since then many workers have measured atmospheric properties using wavelengths from millimetres to metres. Earlier microwave measurements of

atmospheric water vapour are made with the sun as the source of radiation (Staelin, 1966), but later, the atmospheric emission spectrum, was used, which permitted night time observations as well.

The attenuation of microwaves in the 1 to 500 GHz region is shown in Fig 4.1 for two values of total precipitable water 21.0 and 3.4mm (Penzias and Burrus, 1973). Attenuation is mainly caused by two gases, i) oxygen, which has a band of resonance absorption lines in the region 0.5cm, superimposed on a weak continuum, and ii) water vapour, which has a weak absorption line at approximately 1.3 cm and a number of stronger lines below 0.2cm, the far tails of which contribute to the absorption in the centimetre wavelength region. The oxygen absorption dominates over that of water vapour, even though the mass absorption coefficients of the two gases are of the same order of magnitude, as a consequence of the large density ratio of oxygen to water vapour in the atmosphere. The oxygen absorption is associated with a magnetic dipole resonance leading to a series of transitions between fine structure levels of various rotational states of the molecules. The resonance occurs in the region about 60 GHz and

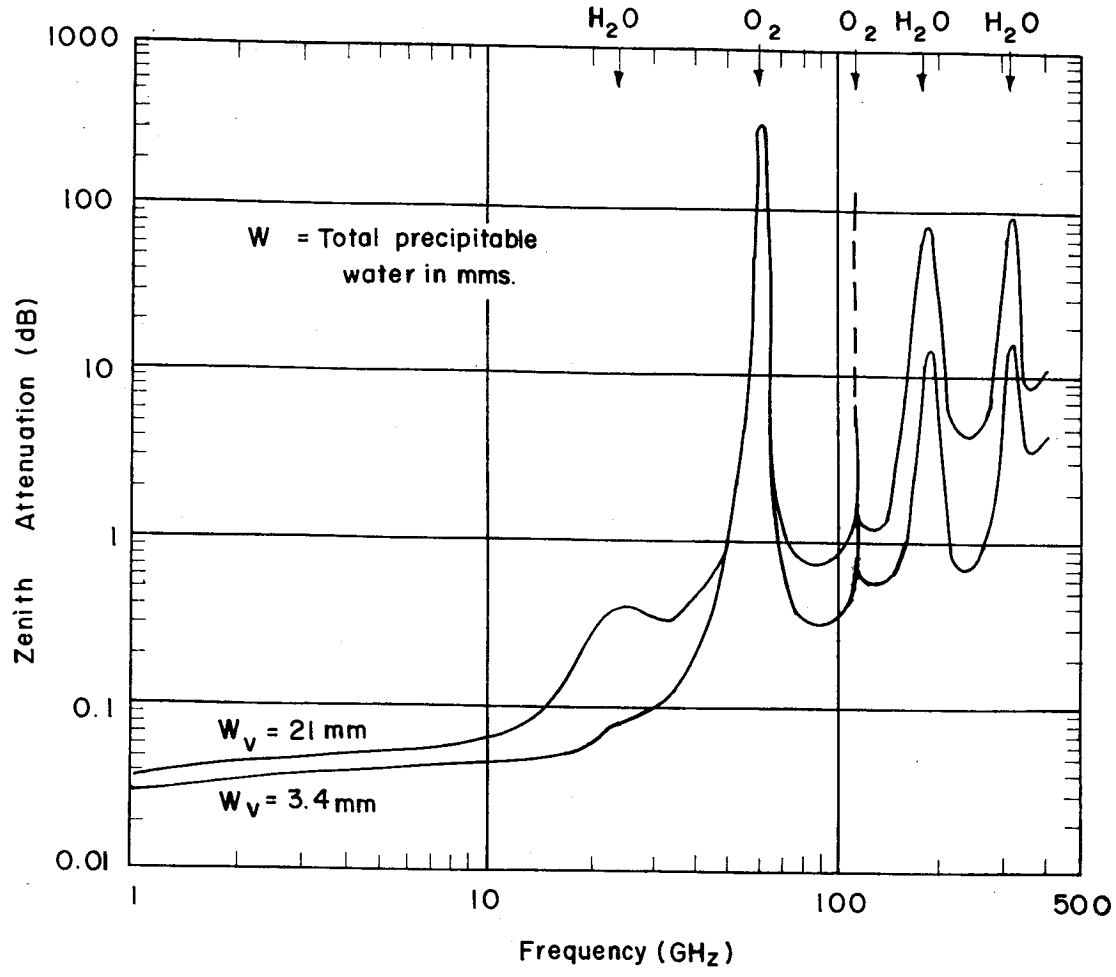

Fig 4.1 Attenuation of microwaves in the atmosphere (Penzias and Burrus, 1973)

118.75 GHz, where there is a single absorption line. The main contribution by water vapour is due to pure rotational transitions at 22.2GHz and 183 GHz and the pressure broadened skirts of absorption lines occuring at submillimetre wavelengths extending well into the infrared. The frequency of such transitions depend upon the energy difference between the levels involved and is given by:

$$\nu_{ij} = \frac{w_j - w_i}{h} \qquad (4.1)$$

where ν_{ij} is the resonant frequency of transition between the energy levels, w_i and w_j are energies of the lower and upper levels respectively and h is Planck's constant. The 1.35 cm water vapour line arises from the transition between quantum levels $5_{2,3}$ and $6_{1,6}$ (Waters, 1976). The quantum numbers are given in $J_{k-1,\ k1}$ notation where J is the total angular momentum quantum number and K-1 and k1 are quantum numbers associated respectively with corresponding states of limiting prolate and limiting oblate symmetric rotors.

4.2 Water vapour molecular absorption

4.2.1 Absorption Coefficient

According to equation (4.1), ν_{ij} is a single

discrete frequency. In actuality the line has a finite width. Because of natural broadening, the Doppler effect and collisions, the transition i-j results in absorption over a band of frequencies. The general expression for the absorption coefficient between the states, i, j, is given by (Waters, 1976)

$$\alpha(\nu)_{ij} = \frac{8\pi^3 N \nu \mu^2}{3hcQ} \left\{ e^{\frac{-E_i}{RT}} - e^{\frac{-E_j}{RT}} \right\} g_i |\phi_{ij}|^2 f(\nu, \nu_{ij}) \qquad (4.2)$$

Here N is the number of absorbing molecules per unit volume, μ the total dipole moment, g_i, the statistical weight of the lower state, ϕ_{ij} the transition matrix element, f (ν , ν_{ij}) a function describing the line shape and Q the partition function. The partition function Q depends upon the symmetry, rotational constant and other properties of the molecule.

The line-shape function f (ν, ν_{ij}) depends upon the mechanism which dominates spectral line broadening. In the lower atmosphere, collisional interaction between absorbing molecules is mainly responsible for

broadening of absorption lines. Two theoretical line shapes have been commonly used. The form proposed by Van Vleck and Weisskopf (1945) is

$$f(\nu,\nu_{ij}) = \frac{1}{\pi}\left(\frac{\nu}{\nu_{ij}}\right)\left\{\frac{\Delta\nu}{(\nu-\nu_{ij})^2+\Delta\nu^2} + \frac{\Delta\nu}{(\nu+\nu_{ij})^2+\Delta\nu^2}\right\} \qquad (4\cdot3)$$

where $\Delta\nu$ is a line width parameter.
That derived by Gross (1955) which is also known as the "kinetic line shape" is

$$f(\nu,\nu_{ij}) = \frac{1}{\pi}\,\frac{4\nu\nu_{ij}\Delta\nu}{(\nu_{ij}-\nu)^2+4\nu^2\Delta\nu^2} \qquad (4\cdot4)$$

The kinetic line shape appears to give results which are more nearly in agreement with experimental data.

The collisional line width parameter $\Delta\nu$ which appears in the above equations is a function of both temperature (T) and pressure (p). Taking into consideration the typical intermolecular force, the temperature dependence has been shown to be:

$$\Delta\nu = \Delta\nu^{o}\left(\frac{p}{p_o}\right)\left(\frac{T}{T_o}\right)^{-x} \qquad (4\cdot5)$$

where x is usually between 0.7 and 1.0 and $\Delta\nu^{o}$ is the value of $\Delta\nu$ at $p = p_o$ and $T = T_o$ (Waters, 1976).

So far, only the absorption due to a single transition has been considered. But a molecule may have many energy levels and hence many allowed transitions. If there is no interaction between the various transitions, and the radiation from different transitions is incoherent, then the total absorption coefficient at any frequency is the sum of the absorption coefficients. Therefore,

$$\alpha(\nu) = \sum_{\text{All transitions}} (\alpha_{\nu'})_{ij} \qquad (4.6)$$

For the water molecule, taking appropriate constants into consideration and using the kinetic line shape, the total absorption coefficient for frequencies below 100 GHz, is given by:

$$\alpha(\nu) = d_v \nu^2 \Delta\nu_1 T^{-3/2} \left\{ \frac{7.18e^{-\frac{644}{T}}}{T} \cdot \frac{1}{(494.4019-\nu^2)^2 + 4\nu^2\Delta\nu^2} + 2.77\times10^{-8} \right\} \text{ cm}^{-1} \qquad (4.7)$$

where $\Delta\nu_1 = 2.96\left(\frac{p}{1013}\right)\left(\frac{300}{T}\right)^{0.626}\left(1+\frac{0.018\, d_v T}{p}\right)$ GHz

ρ_v is in g m^{-3}, T in degree Kelvin, p in millibars, and ν in GHz (Waters, 1976). This expression includes an empirical correction term to make the computed value agree with the experimental value.

The absorption coefficient $\alpha(\nu)$describes the interaction of radiation with the absorbing matter (water vapour), as discussed above. It is in general a function of water vapour density, temperature and pressure of the atmosphere, all of which vary along the path of observation.

Downward transitions between the energy states of the water vapour molecules cause them to radiate energy in the same frequency intervals as those of radiowaves that could be absorbed by these molecules. The magnitude of this emission is governed by the absorption coefficient $\alpha(\nu)$. When a radiometer is working in the emission mode, without a background source in its beam, it is receiving this incoherent noise-like radio energy emitted by water vapour molecules dispersed in that part of the atmosphere within the beam.

4.2.2 Equation of radiative transfer

At the wavelengths of interest here, Planck's

radiation formula reduces to Rayleigh-Jean's law which is expressed as:

$$P = \frac{2kT\nu^2}{c^2} \cdot \Delta\nu \cdot d\Omega \qquad (4.8)$$

where P = power radiated into solid angle $d\Omega$, in band width $\Delta\nu$,

h = Planck's constant,

ν = frequency,

c = velocity of light,

k = Boltzmann constant, and

T = Temperature in ^{o}K.

The microwave water vapour radiometer consists of a directional antenna pointed at the sky and connected to a special microwave receiver, which measures the thermal radiation intercepted by the antenna. It is convenient to consider this radiation as originating in the effective terminating impedance of the antenna and to assign to this impedance, a thermodynamic temperature T (^{o}K), that the corresponding "Johnson noise" is equal to the observed radiation. If the radiation intercepted by the antenna is P ergs/sec, in the frequency range $\Delta\nu$ cycles/sec, this temperature is $T = P\,(k\,\Delta\nu)^{-1}\ ^{o}K$ (4.9).

This will be called the noise temperature of the antenna or simply the antenna temperature. The relation between the antenna temperature and the atmospheric radiation processes is discussed in the following paragraphs.

The power incident on the antenna from any given direction can be described by a brightness temperature $T_B(\nu, \theta, \phi)$. The antenna temperature is then an average of brightness temperature weighted over 4π steradians according to the gain function $G(\nu, \theta, \phi)$. That is,

$$T_A(\nu) = \frac{1}{4\pi} \int_{4\pi} T_B(\nu, \theta, \phi)\, G(\nu, \theta, \phi)\, d\Omega \qquad (4.10)$$

If $T_B(\nu)$ is assumed to be constant over the main beam and side-lobes are neglected, we have $T_A(\nu) = T_B(\nu)$ which is nearly the situation for a ground based radiometer looking at the zenith without any background source in its beam.

The brightness temperature T_B (or T_A) observed is related to the atmospheric composition and temperature T (Z) along the line of sight and T_{bg} the brightness

temperature due to cosmic background radiation. To an excellent approximation, the equation is,

$$T_A(\nu) = T_B(\nu) = T_{bg} e^{-\tau(\nu)} + \int_0^\infty T(z)\alpha(z) \exp\left[-\int_0^z \alpha(z)dz\right] dz \qquad (4.11)$$

where, $T_A(\nu)$ is the observed antenna temperature of a radiometer looking up at the zenith, $\alpha(z)$ is the absorption coefficient for ν at a height z, and,

$\tau(\nu) = \int_0^\infty \alpha(z)\,dz$ is the optical depth.

Here the scattering and refractive index variations are neglected and thermal equilibrium in the atmosphere is assumed, and both these are true for molecular absorption at microwave frequencies. The equation (4.11) expresses the fact that the brightness temperature in a direction is the sum of the background radiation attenuated by the whole atmosphere and the radiation emitted at each point along the path, each component being attenuated by the intervening atmosphere. Fig 4.2 illustrates these various contributions

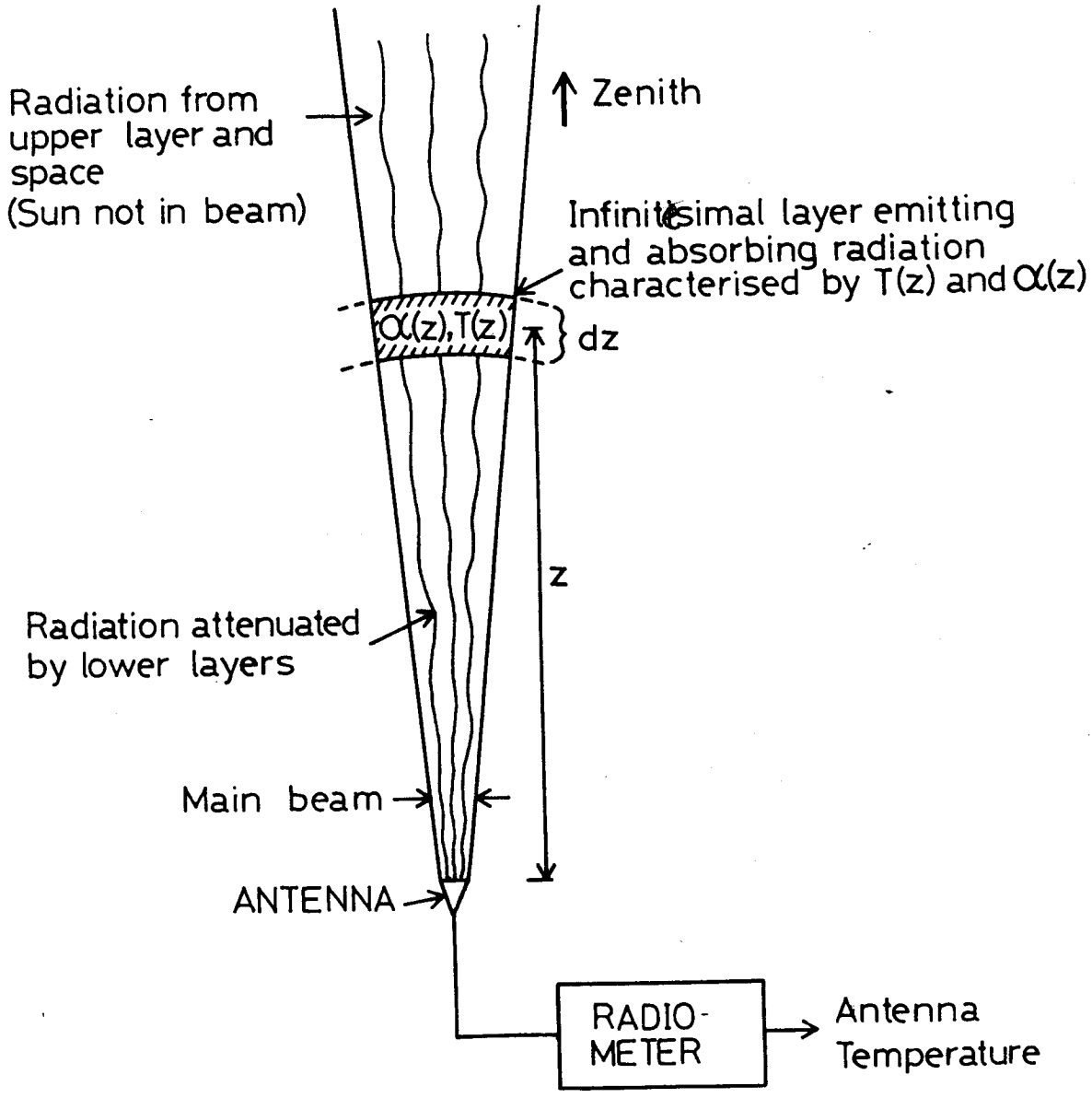

Fig 4.2 Ground based microwave radiometer sensing the atmospheric emission (Rainwater, 1978)

to the energy received by a ground based radiometer (Rainwater, 1978).

If T (Z), the temperature of atmosphere is assumed to be the same T_o throughout, equation (4.11) is simplified to

$$T_A(\nu) = T_{bg}\, e^{-\tau(\nu)} + T_o\,(1 - e^{-\tau(\nu)}) \qquad (4.12)$$

Thus, the T_A measured by a radiometer working at the water vapour resonance line, in the emission mode, depends on τ , the atmospheric opacity due to water vapour, which in turn depends upon the water vapour content. Therefore, T_A is an indicator of precipitable water W. However, it is necessary to assign some value to T_o for the atmosphere, which must be obtained by other means.

4.3 Principle of the microwave water vapour radiometer

4.3.1 General

The basic function of a radiometer is to measure the radiant power absorbed by the antenna. For a receiver with a bandwidth B, the power delivered at its input, neglecting losses in the transmission line

between the antenna feed and receiver input, can be expressed in terms of an antenna temperature as follows:

$$W_s = kT_A B \tag{4.13}$$

where W_s = antenna noise power

k = Boltzman constant

T_A = antenna temperature

B = bandwidth

But the receiver also contributes noise due to thermal and other noise in the receiver components such as the transistors. Therefore, the total system noise power at the antenna terminals is:

$$W_{sys} = W_s + W_R = K\,(T_A + T_R)B$$

$$\text{Or} \quad T_{sys} = T_A + T_R \tag{4.14}$$

where W_R is the receiver noise power referred to the antenna terminals, and T_R is the receiver noise temperature.

It is clearly desirable that T_R should be as small as possible.

Another important parameter of a radiometer is its

senstivity. It is the minimum detectable signal and is defined as the signal that causes a deflection at the receiver output equal to the standard deviation (r.m.s.) of the output fluctuations about the mean. It can be shown (Kraus, 1966) that the standard deviation ΔT of the output about the mean of the radiometer system is given by:

$$\Delta T = \frac{T_{sys}}{\sqrt{Bt}} \qquad (4.15)$$

where T_{sys} is the total system temperature

B is the predetection effecive bandwidth, and

t is the true integration time at the receiver output.

The above expression for system sensitivity holds good for an ideal case when receiver gain and bandpass characteristics are constant. However, in practice, because of supply voltage and temperature variations, this is not true. Generally, such instabilities set the limit on sensitivity in an actual system.

There are basically two types of radiometers: the total power radiometer and the Dicke comparison radiometer (1946).

In the absence of gain, bandwidth and noise temperature variations, the total power receiver has the maximum possible sensitivity. In practice, however, achieving adequate stabilisation of these variables is very difficult. Most of these difficulties can be overcome by the use of the comparison radiometer technique at microwave frequencies (Dicke, 1946).

4.3.2 Dicke's Comparison Radiometer

It has been shown that the spectrum of gain fluctuation in amplifiers decreases rapidly with frequency. In the Dicke system, the input of the receiver is rapidly switched between the antenna and a comparison or reference noise source. The switching is at a frequency high enough so that over a period of one switching cycle, the low frequency gain variation is hardly noticeable. After conversion, amplification and detection, the modulated signal is passed through a synchronous demodulator that produces an output voltage proportional to the difference in power (or temperature) between the reference and signal inputs. The block diagram of a Dicke's radiometer system is shown in Fig 4.3.

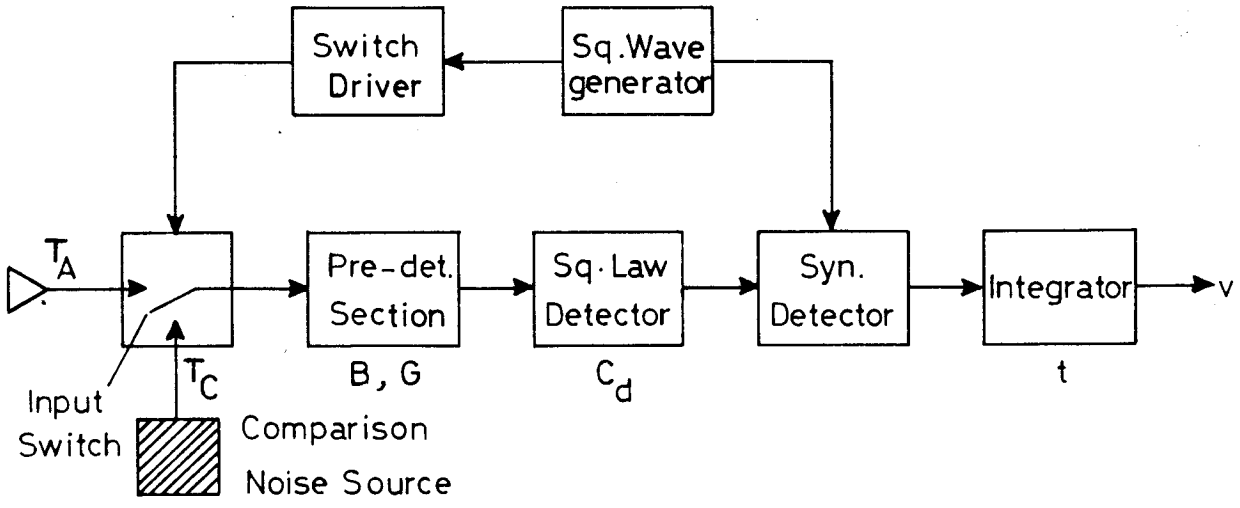

Fig 4.3 Block diagram of Dicke's radiometer system

If B is the predetection effective bandwidth, G, the predetection power gain, c_d, the square-law detector power sensitivity (volts/watt), and t the integration time,

the integrator output $v = g C_d G k B (T_A - T_c)$

$$v = GK (T_A - T_c) \qquad (4.16)$$

where g is the post-detection voltage gain and $K = g C_d kB$. If the difference $(T_A - T_c)$ is kept small, say a few per cent of the system temperature, the effect of gain changes on the output and hence on sensitivity is reduced. It can be shown that in this case receiver sensitivity is given by (Moore, 1975)

$$\Delta T = (T_A + T_c + 2T_R)\left[\frac{1}{Bt} + \left(\frac{\Delta G}{G}\right)^2\left(\frac{T_A - T_c}{T_A + T_c + 2T_R}\right)^2\right]^{1/2} \qquad (4.17)$$

Most of the microwave radiometers used for the purpose of observing atmospheric attenuation or in remote sensing of the earth from satellites are Dicke receivers.

4.3.3 Application of microwave radiometry in the remote sensing of the atmosphere

The technique of passive microwave radiometry was first applied to observe the earth's atmosphere in 1946 by Dicke and his associates (1946). Their measurements were part of an investigation of the 1.35 cm water vapour line and were realized through the use of the "switched receiver" concept. Since then, this technique has been widely adopted in radio astronomy, meteorology and also in studying the microwave attenuation properties of the atmosphere. Barret and Chung (1962) and Staelin (1966) have discussed the determination of profile information from multispectral emission or extinction observations. Staelin (1966) used his five channel radiometer for measurements at and near 22 GHz in solar radiation extinction experiments. These observations showed that measurements of microwave spectra of atmospheric opacity near the 22 GHz line can yield information about the total precipitable water and its distribution with altitude. More recently, the Wave Propagation Laboratory of the National Oceanic and Atmospheric Administration (NOAA) has constructed a dual-channel system at 20.6 and 31.65 GHz (Guiraud et al, 1979) for measuring total integrated water vapour and cloud liquid. In all of

these experiments, radiosonde data were used to calibrate and evaluate the performance of radiometers. There are presently numerous microwave radiometers working in different countries all over the world. All these, together with those operating in earth-orbitting satellites, are probing meteorologically interesting atmospheric conditions at different microwave frequencies from 3 GHz to 300 GHz.

4.4 Description of the Microwave Watervapour Radiometer (MWR)

4.4.1 Description of the system

The microwave water vapour radiometer on its stand is shown in Fig 4.4. Figs 4.5 and 4.6 show two views of the instrument with the cover removed. The radiometer operates in a frequency comparison mode where the emission from the atmosphere in the two frequency bands 22.24 GHz and 20.5 GHz are compared. The block diagram of the water vapour radiometer is shown in Fig 4.7. The high frequency section of the instrument consists of a horn antenna, local oscillators, mixer-cum-preamplifier, IF amplifiers, filter, gain modulating system, noise source and detector. The low frequency section of the circuit consists of a square wave generator, switch driver, D.C. bias supply for the oscillators, D.C. amplifier, synchronous

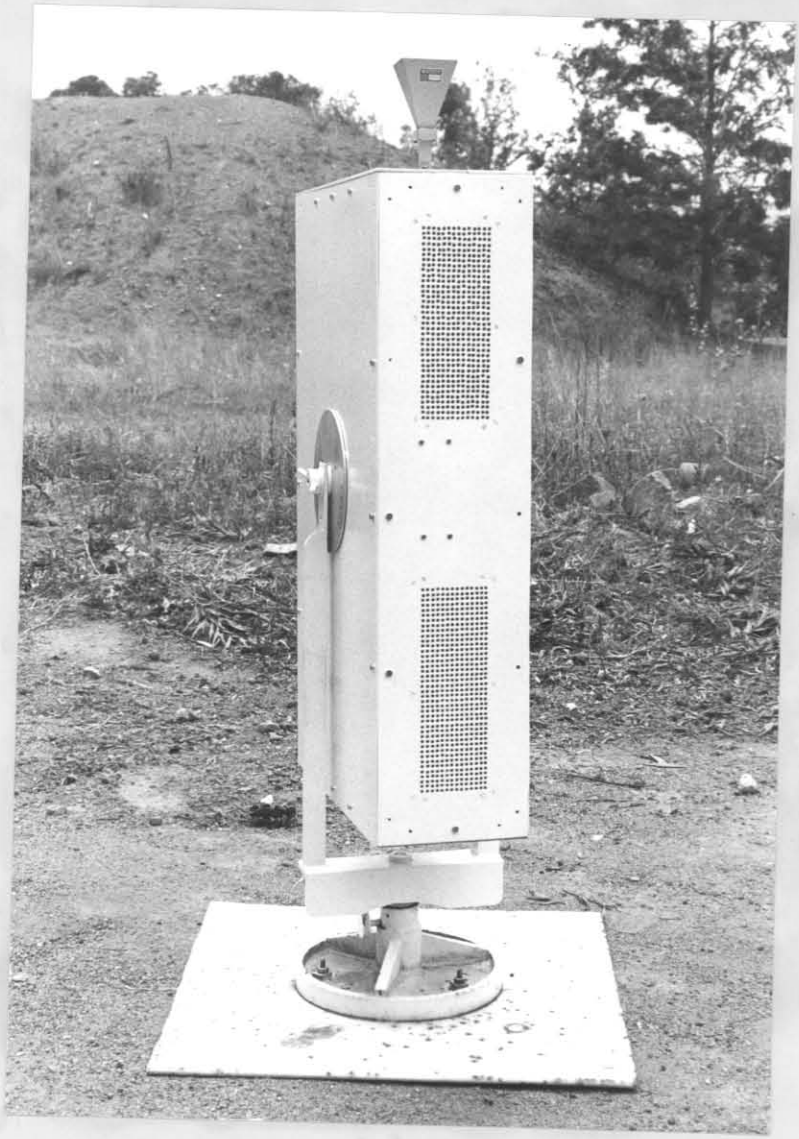

Fig 4.4: Photograph of the microwave water vapour radiometer.

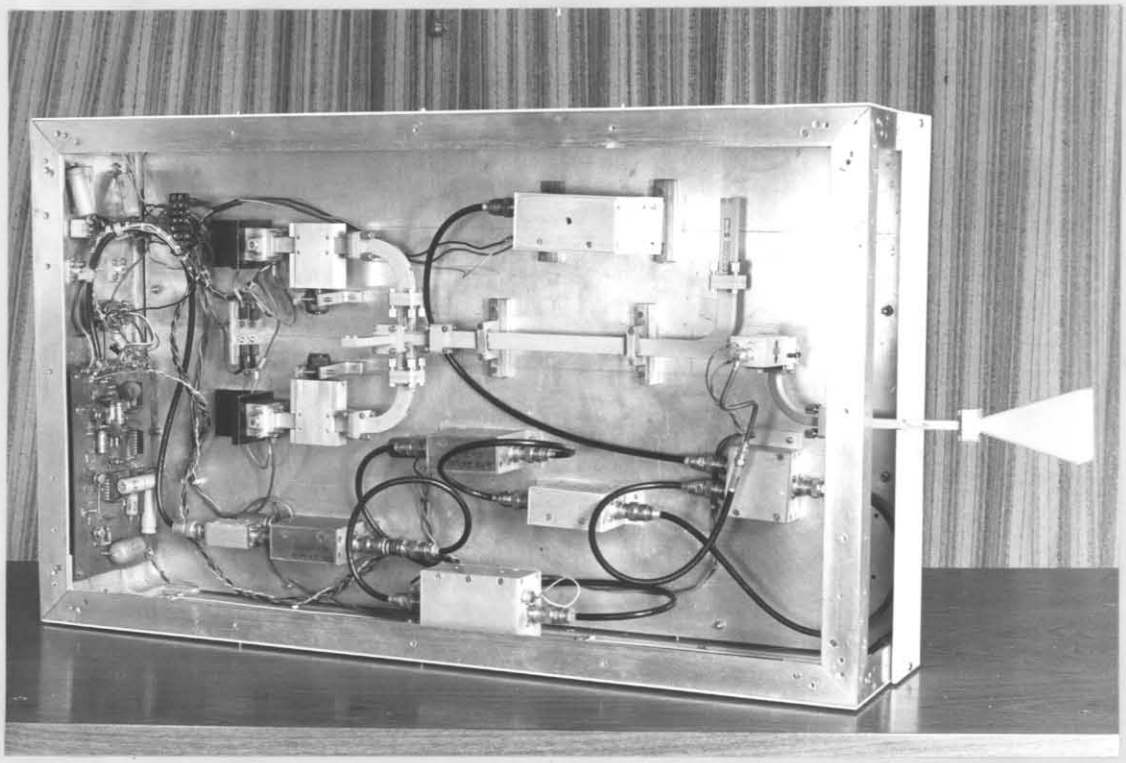

Fig 4.5: Photograph of the microwave water vapour radiometer with cover removed.

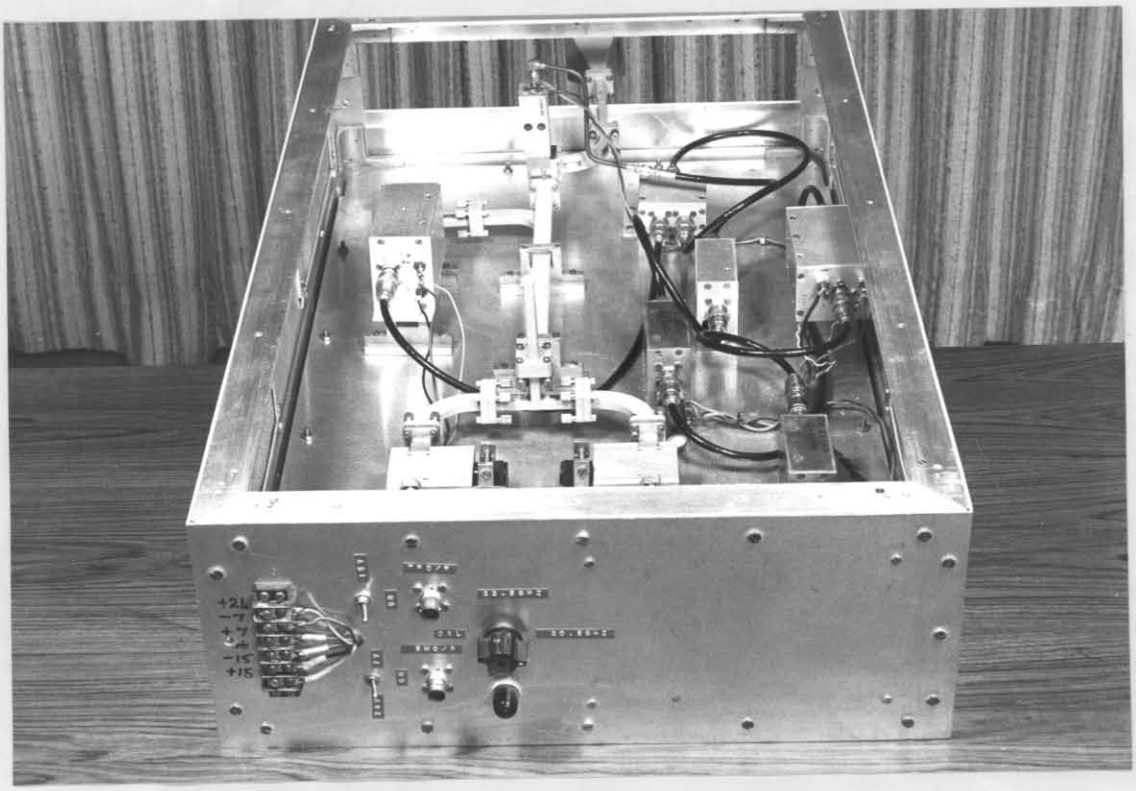

Fig 4.6: Photograph of another view of microwave water vapour radiometer with cover removed.

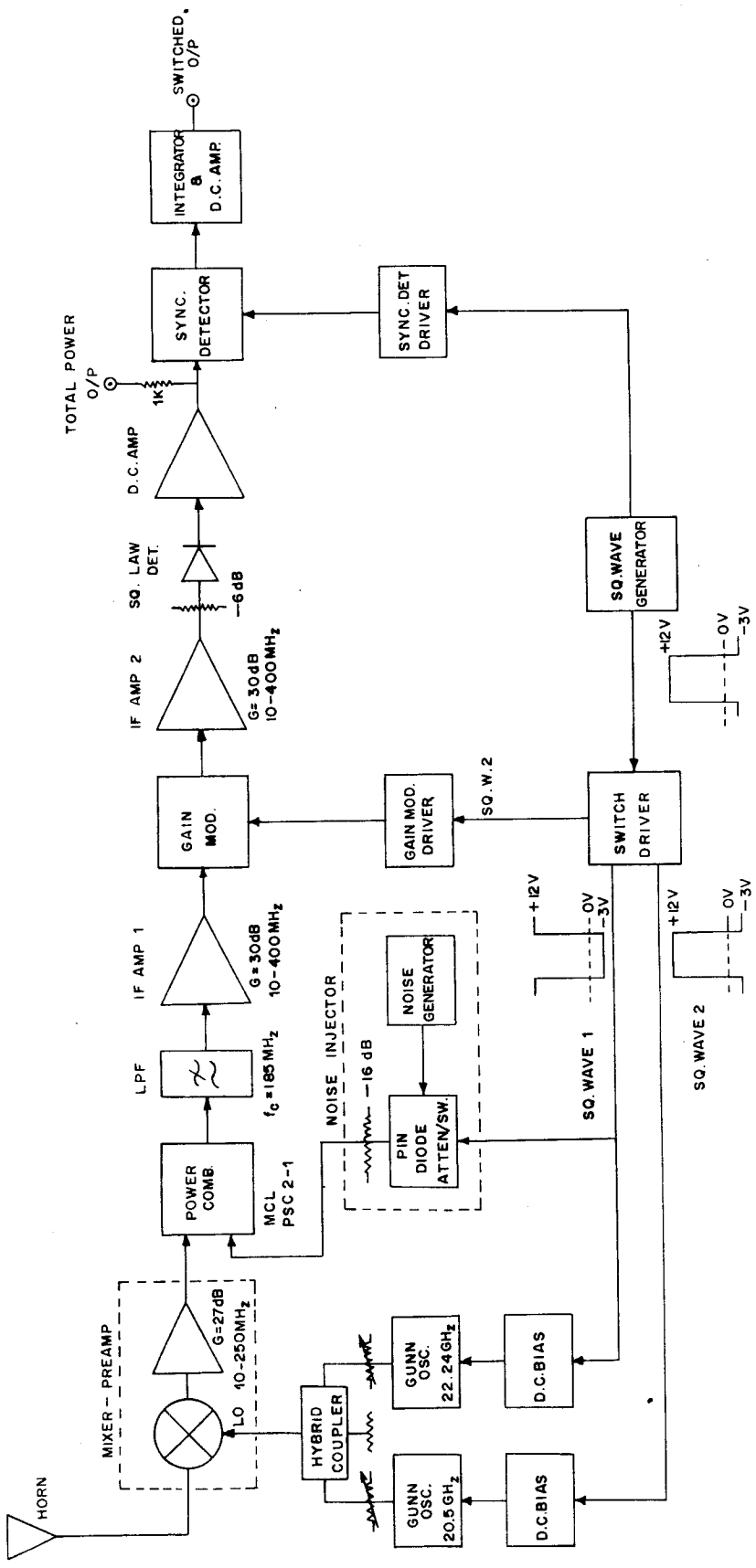

Fig 4.7 Block diagram of water vapour radiometer

detector and integrator. Figs 4.7-4.14 show the details of the circuits.

4.4.1.1 Antenna

The source is the continuous medium, the dispersed water vapour in the atmosphere. Hence, resolution, is of little concern. A K-band horn antenna is used. It has a 3 dB beamwidth of about 15^{o} (G = 20 dB). Since the radiation from the source fills the antenna beam, the antenna temperature is equal to the brightness temperature, if the side lobes and the variation of optical depth within the main beam are neglected.

4.4.1.2 Frequency Switching

In this mode of working, two local oscillators are switched on alternately at a rate of 10 Hz so that only one of them is on at a time. If we think of the system as a Dicke switching system, the reference load is the nearby point (to the signal point) on the spectrum of the source. The signal frequency is 22.24 GHz, the centre of the water vapour resonance line. Ideally, the other should be completely outside the resonance line so that the instrument is sensitive to small variations in water vapour content. But this is impractical due to the large width of the spectralline $\smile$8 GHz.

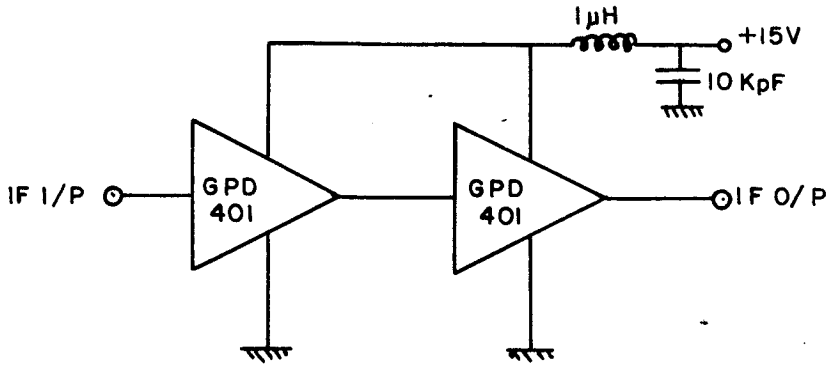

IF AMP 1

G = 30dB

−1 dB FREQ. RESPONSE 10 −400 MH_z.

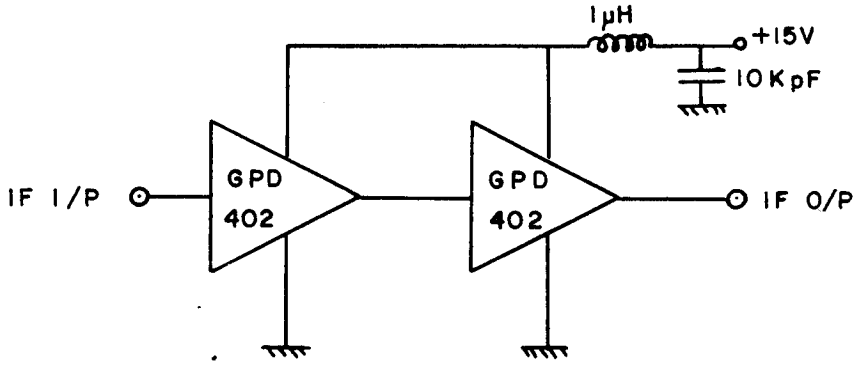

IF AMP 2

G = 30dB.

−1dB FREQ. RESPONSE 10 − 400 MH_z

Fig 4.8 I F Amplifiers

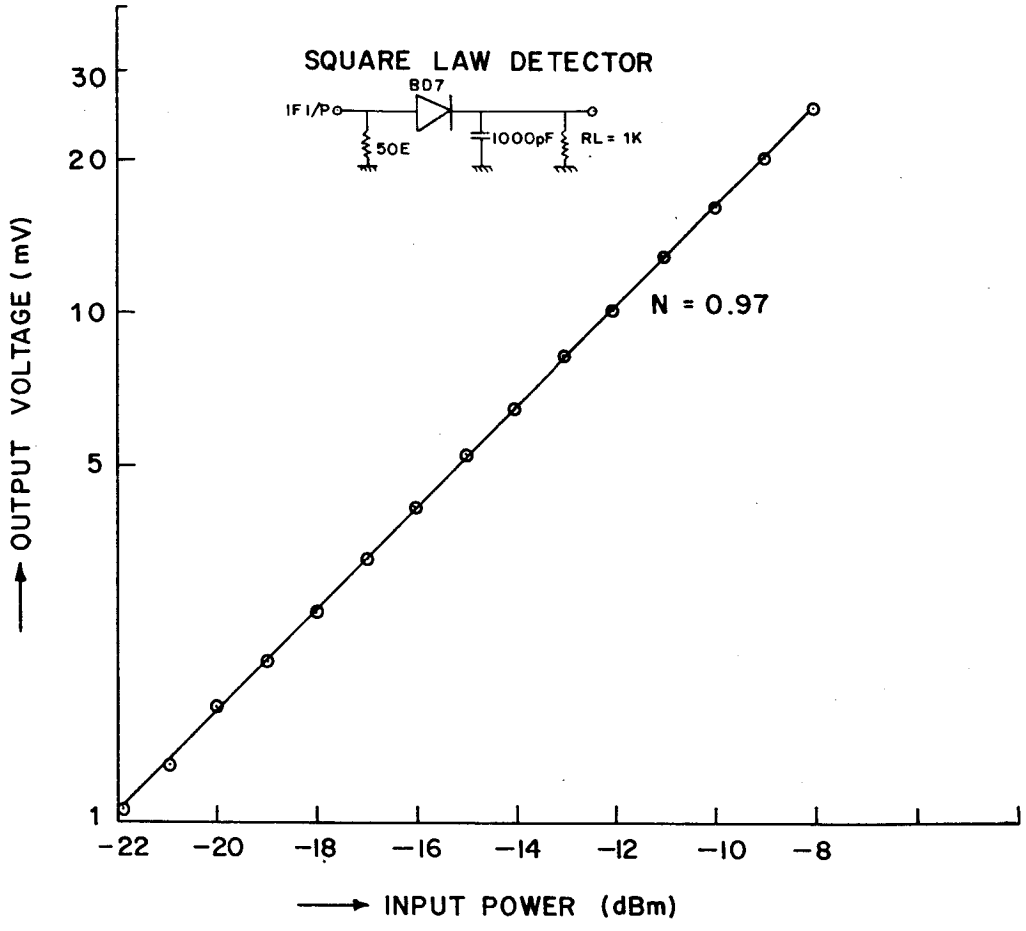

Fig 4.9 Circuit diagram of square law detector and its characteristics

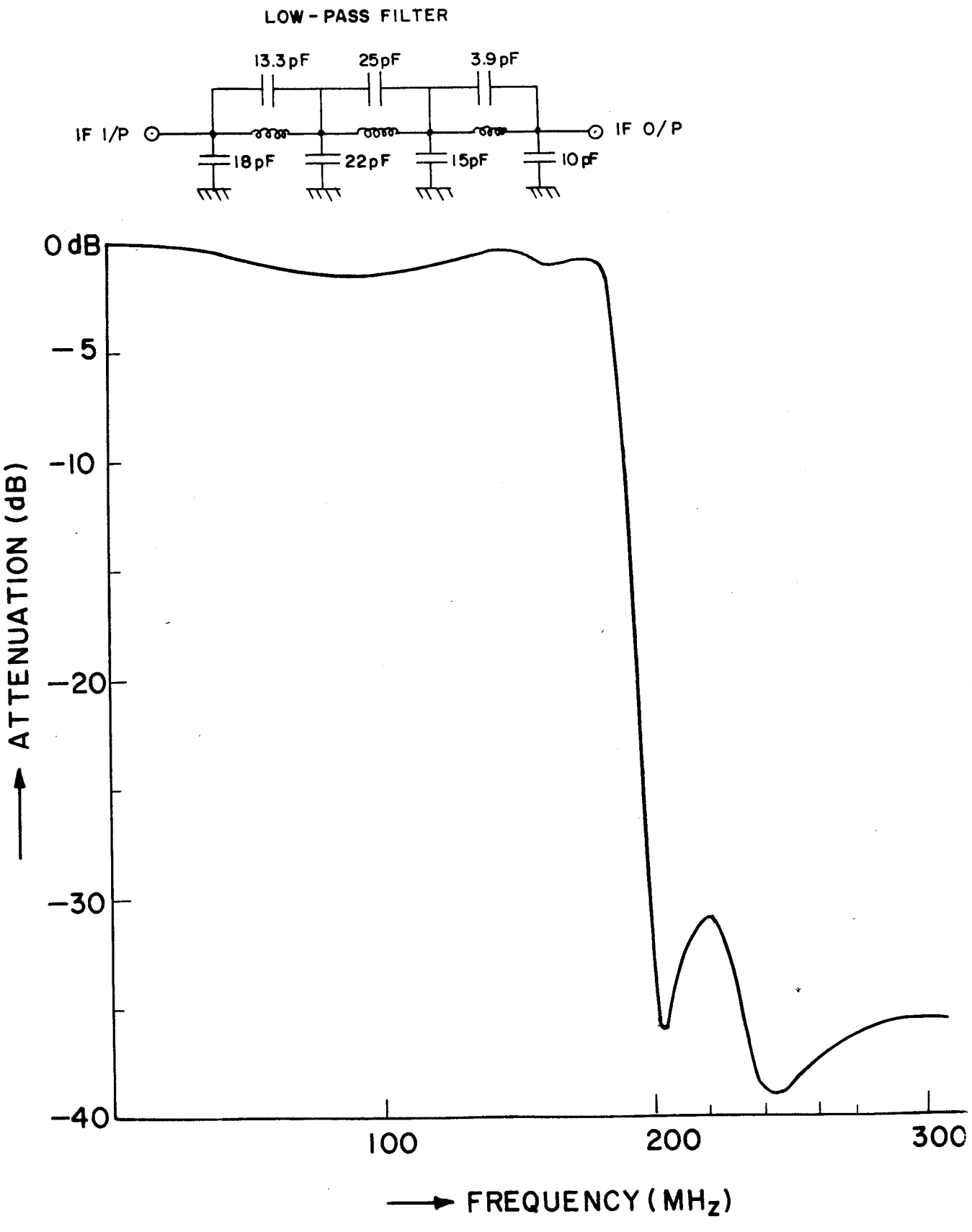

Fig.4.10 Circuit diagram of low-pass filter and its characteristics

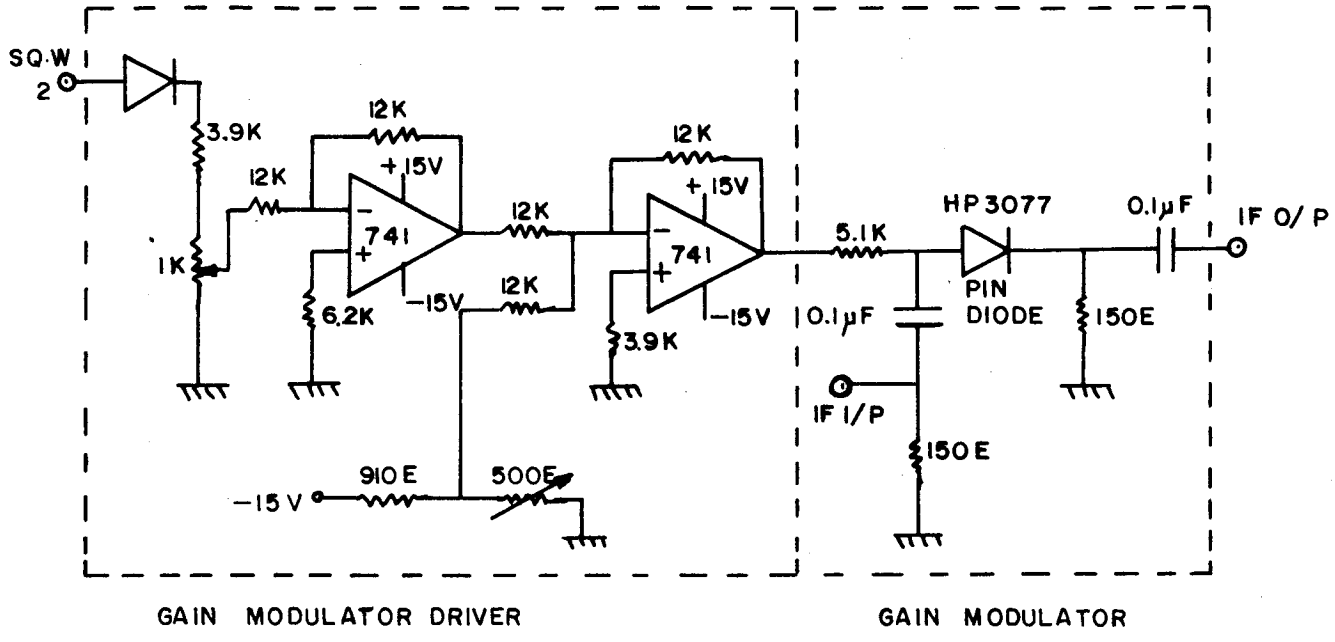

Fig.4.11 Circuit diagram of gain modulator

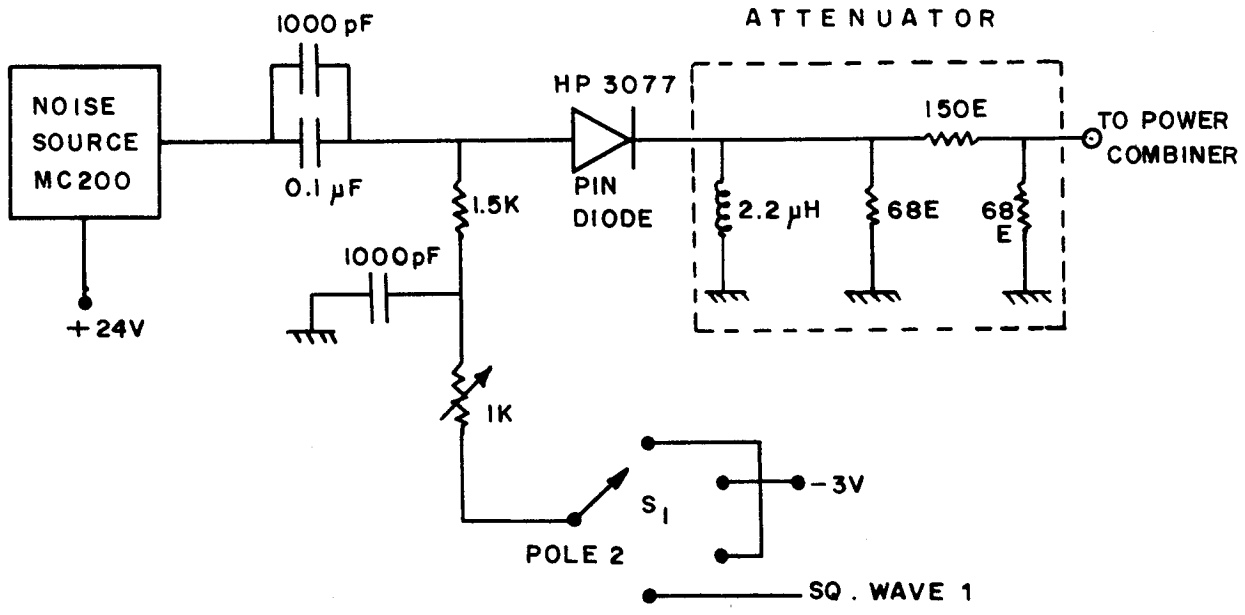

Fig. 4.12 Circuit diagram of noise injection scheme

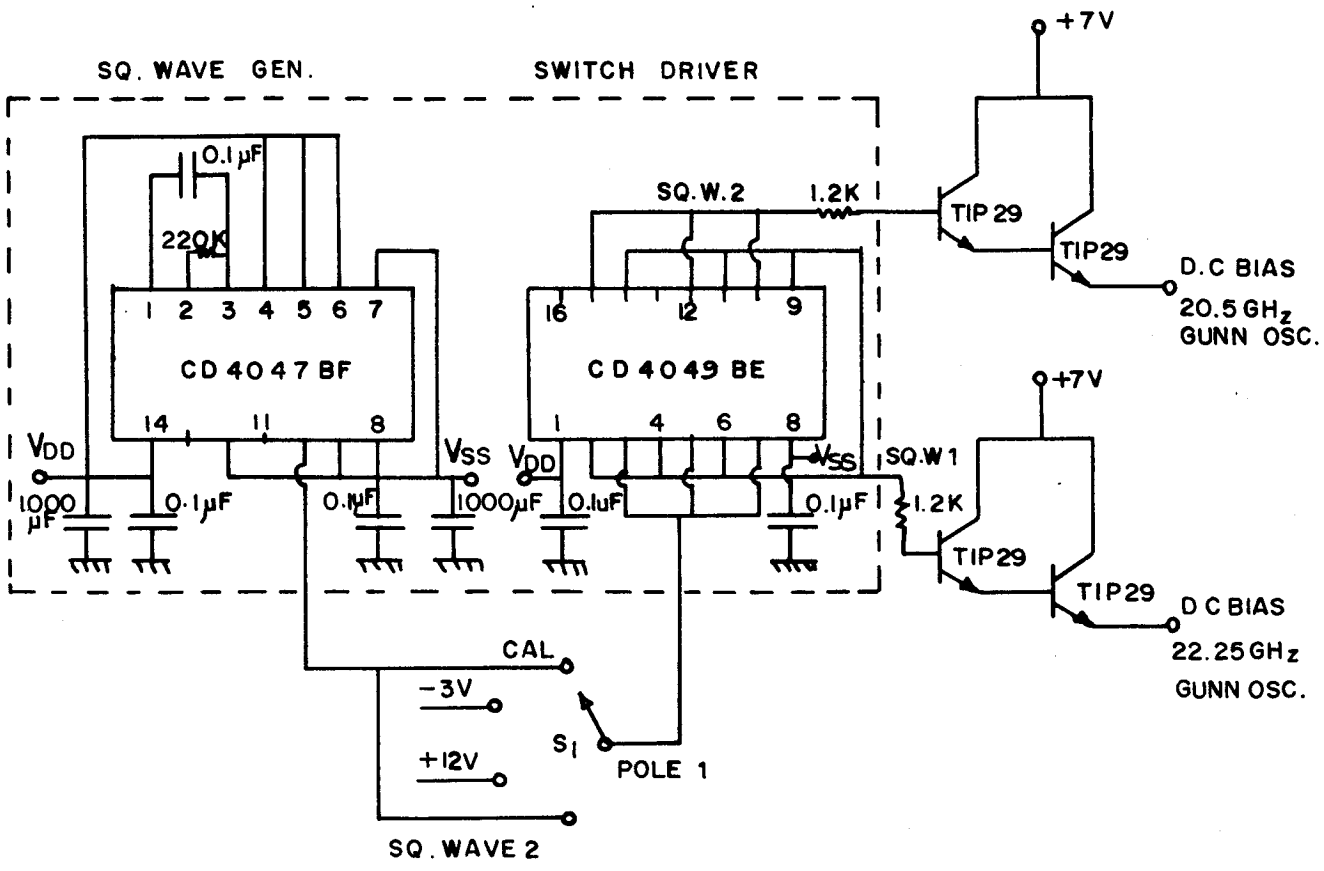

Fig. 4.13 Circuit diagram of square wave generator, switch driver and bias supply for Gunn oscillators

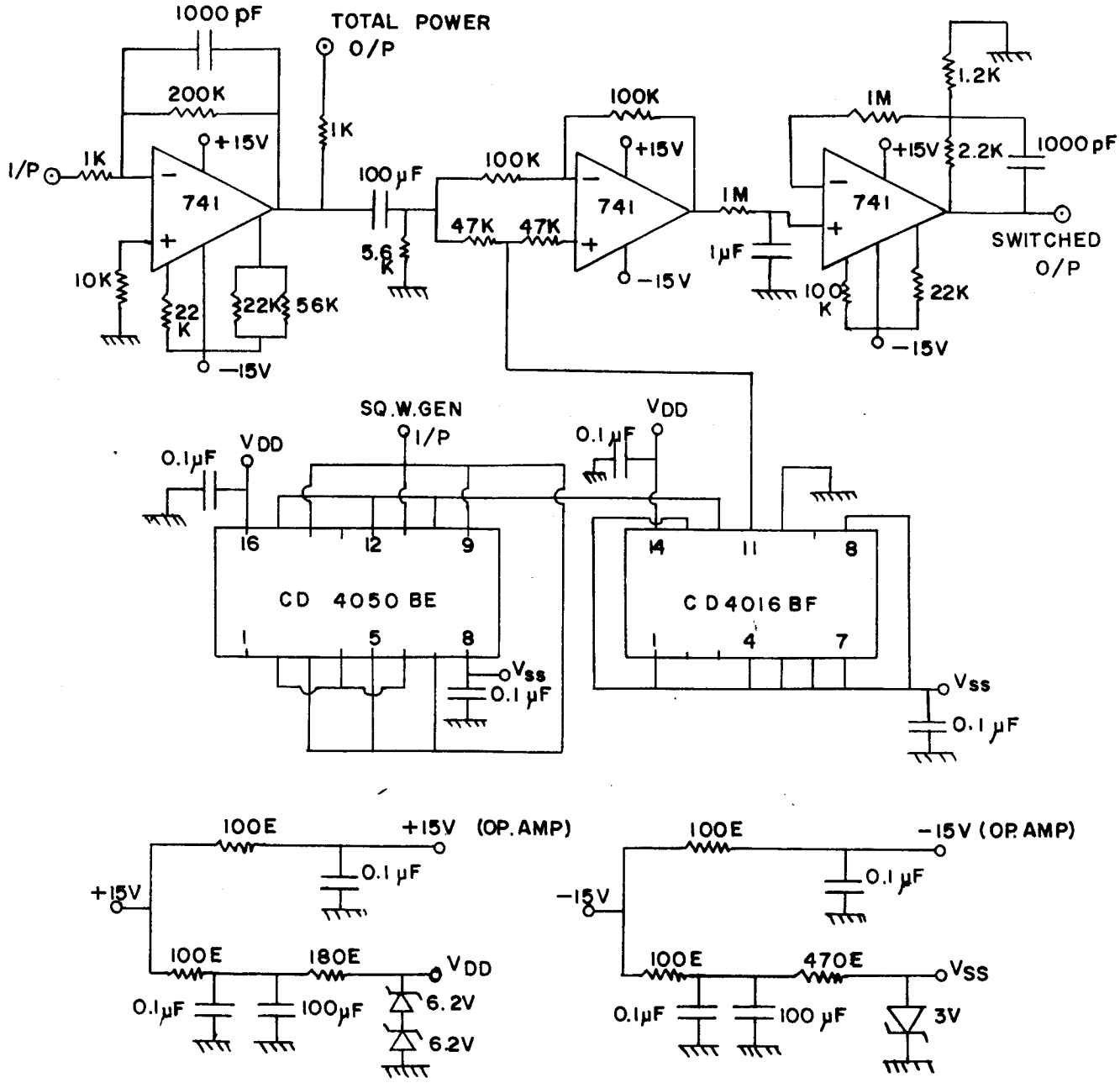

Fig. 4.14 Circuit diagram of the synchronous detector

Therefore, 20.5 GHz was selected as the other frequency so that the spectral response of the front end components can accommodate both frequencies. However, there is some loss in sensitivity because the reference frequency lies on the wing of the line. On the other hand, contributions from the dry components and liquid water (clouds) is eliminated to a large extent, as is the effect of ground radiation through side lobes. Equation (4.16) now becomes,

$$v = G_1 k\left[T_{R1} + T_1 + T_{sp}\right] - G_2 k\left[T_{R2} + T_2 + T_{sp}\right] \qquad (4.18)$$

where T_1 and T_2 are antenna temperatures, T_{R1}, T_{R2} are noise temperatures, and G_1, G_2 are the gains corresponding to 22.24 GHz (f_1) and 20.5 GHz (f_2) respectively. T_{sp} = spillover temperature assumed to be the same at the two frequencies.

4.4.1.3 Gain modulation

By using current controlled attenuators in the IF stage, the overall IF gains are made equal ($G_1 = G_2 = G$) for the two frequencies. Thus equation (4.18) becomes,

$$v = GK\ (T_1 - T_2) + GK\ (T_{R1} - T_{R2})$$

$$v = GK\ (T_1 - T_2 + T_{R1} - T_{R2}) \qquad (4.19)$$

4.4.1.4 Noise addition

As can be seen from the above equation, the variation in switched output, because of gain variations due to instabilities, can be reduced by making the bracketed quantity still smaller. This is accomplished by adding IF noise from a broadband noise source in one of the channels. The amount of added noise is so adjusted that,

$$GK \left[T_{R1} - T_{R2} + \frac{T_n}{G'} \right] = 0 \qquad (4.20)$$

where T_n is the added noise in the IF stage and G' is the IF gain before the power combiner stage. Equation (4.19) becomes,

$$v = GK (T_1 - T_2) \qquad (4.21)$$

4.4.1.6 Receiver sensitivity

Using equation (4.17), the receiver sensitivity T can be determined. In this case $T_A = T_1$, $T_C = T_2$,

$2T_R = T_{R1} + T_{R2} \simeq 1200\ ^oK$

Taking $T_1 + T_2 + 2T_R \simeq 1300\ ^oK$

$B = 185 \times 10^6$ Hz, $t = 1$ sec.,

the ideal value of receiver sensitivity $\Delta T = 0.1^oK$.

If the variation in G is taken to be 2%, ΔT comes out to be $\sim .5^{o}K$ from equation (4.17).

4.4.2 Principle of measurement

We have, from equation (4.12), taking $T_A(\nu) = T_1$ corresponding to 22.24 GHz,

$$T_1 = T_{bg} e^{-\tau_1} + T_o (1 - e^{-\tau_1})$$

$$= T_o + (T_{bg} - T_o) e^{-\tau_1} \qquad (4.22)$$

where T_{bg} = Cosmic background radiation temperature

T_o = Mean atmospheric temperature

τ_1 = Optical depth for f_1, due to water vapour

and $T_2 = T_o + e^{-\tau_2} (T_{bg} - T_o)$

Therefore $T_1 - T_2 = (T_o - T_{bg})(\tau_1 - \tau_2)$ (4.23)

assuming τ_1 and τ_2 to be small, T_{bg} could be neglected in comparison with T_o. Thus knowing or assuming the value for T_o, $(\tau_1 - \tau_2)$ can be found from the observed value of $T_1 - T_2$ from the radiometer.

If an average value for $\frac{\tau_1}{\tau_2}$ is assumed or an

approximate value is estimated by total power observations, τ_1 and τ_2 can be determined. These values may include a small contribution from oxygen and other trace molecules and also a side-lobe contribution effect. By knowing the actual values of W corresponding to several values of $T_1 - T_2$, a calibration curve can be obtained which would directly give W for any value of $T_1 - T_2$.

4.4.3 Operation of the microwave water vapour radiometer

The detailed operation of the radiometer can be understood by referring to Fig 4.7. A square wave of frequency of about 10 Hz is produced by the square wave generator. From this two sharp square wave trains SQ.W.1 and SQ.W.2 out of phase with each other, as indicated in the Fig 4.7 are derived through the switch driver. Each of these drives the base of a Darlington pair of TIP 29 transistors and provides square waves of required bias voltage for the Gunn oscillator. These turn the two LOs on alternately. The LO powers are controlled by attenuators in the waveguide and fed to the mixer through a hybrid coupler. RF signal power is coupled to the mixer through the waveguide by the horn antenna. The IF output from the mixer preamplifier is fed to a power combiner through a coaxial cable.

Into the other input port, noise is injected during the interval when the signal corresponding to f_1 is present in the channel. The IF signal is bandshaped by a low-pass filter. This bandshaped IF signal next passes through IF AMP1. The following stage is the gain modulation unit. IF AMP2 amplifies the signal and feeds it to the square law detector through a 6 dB attenuator. The detector output is amplified by a D.C. amplifier which is followed by the synchronous detector integrator and the last amplifier. The radiometer output is fed to a chart recorder.

4.4.4 Noise measurement

The LO frequencies are set at 22.24 GHz and 20.5 GHz and the powers are equalised. The gains of the two IF channels are equalised (i.e. $G_1 = G_2 = G$).

For determining T_R's, absorbers at room temperature and at liquid air temperature are used as standard sources covering the horn, the noise source being turned off. Let T_H and T_C be the room and liquid air temperatures. Then, in the total

power mode, we have for frequency f_1, the equation

$$GK \ (T_{R1} + T_H) = V_H \tag{4.24}$$

and $GK \ (T_{R1} + T_C) = V_C$ (4.25)

where V_H and V_C are the total power outputs for f_1.

From the above relations

$$T_{R1} = \frac{T_H - T_C}{Y - 1} - T_C \tag{4.26}$$

where $Y = \frac{V_H}{V_C}$

In the same way T_{R2} is also determined. The T_R's were determined inside the laboratory as well as at the place where the radiometer was actually in operation. These measurements were made periodically. While the value of T_R'S were somehwat variable, $T_{R1} - T_{R2}$ however, was fairly constant at 130°K with a maximum uncertainty of about ± 5°K. T_{R1} and T_{R2} were around 500°K and 625°K.

4.4.5 Gain calibration

In the total power mode, with the absorber at room temperature covering the horn, since $G_1 = G_2 = G$,

and the noise source is off, we have for f_1,

$$GK \ (T_{R1} + T_H) = V_1 \qquad (4.27)$$

and for f_2,

$$GK \ (T_{R2} + T_H) = V_2 \qquad (4.28)$$

In the switching mode of operation of the radiometer, and with the absorber as in the previous case, we have, from the above two equations,

$$GK \ (T_{R1} - T_{R2}) = V_1 - V_2 = V_{cal}$$

where V_{cal} is the corresponding output (mV)

$$\text{Therefore, } GK = \frac{V_{cal}}{(T_{R1} - T_{R2})} \ (mv/^oK) \qquad (4.29)$$

and is thus a determination of the gain.

4.4.6 $(T_1 - T_2)$ from the radiometer output

4.4.6.1 In the normal (switched) mode of working, the noise source is on during alternate half periods. With the room temperature absorber over the horn, we have for this situation,

$$GK\left(T_{R1} + \frac{T_n}{G'} + T_H\right) - GK\left(T_{R2} + T_H\right) = V_H$$

i.e., $GK\ (T_{R1} - T_{R2} + \frac{T_n}{G'}) = v_H$ (4.30)

where v_H is the corresponding output (mv)

It is to be noted that magnitude of T_n is adjusted so that v_H is very small.

If the absorber is now removed and the horn pointed at the sky, we have,

$$GK\ (T_{R1} + \frac{T_n}{G'} + T_1) - GK\ (T_{R2} + T_2) = v$$

i.e.

$$GK\ (T_{R1} - T_{R2} + \frac{T_n}{G'}) + GK\ (T_1 - T_2) = v \quad (4.31)$$

where v is the output of the radiometer (mV).

Substituting 4.30 in 4.31 and rearranging we get,

$$T_1 - T_2 = \frac{v - v_H}{GK} \quad (4.32)$$

Since GK is known from equation 4.29, $(T_1 - T_2)$ is calculated using the noted values of v and v_H.

Taking into consideration various sources of error, it is estimated that the R.M.S. error in the measurement of $(T_1 - T_2)$ is of the order of 10% and somewhat more for lower values of $(T_1 - T_2)$ $(< 5^{\circ}K)$.

The observed ΔT from the chart was generally about

0.3K as against the theoretically expected value of $\sim$0.1K.

4.4.6.2 Side lobe contributions

The pyramydal horn used has side-lobes and their levels are as follows:

E plane first side lobe is 9.1 dB down at 22^{o}

H plane first side lobe is 14 dB down at 28^{o}

E plane second side lobe is 15.4 dB down at 44^{o}

H plane second side lobe is 20 dB down at 45^{o}

Even though the ground radiation entering into the horn through the side lobes gets cancelled when switching between the two frequencies, the sky contributions at the two frequencies do not get cancelled. In the direction of a side lobe, the effective optical depth will be more than the zenith value because of the larger air mass, but the response of the antenna is very much smaller. The net effect is a small contribution due to the side lobes. A rough estimate shows that the effective optical depth for both the frequencies is about 12% more. Therefore, the observed $T_1 - T_2$ and hence $(T_1 - T_2)$ is about 12% larger than the true value.

4.4.6.3 Oxygen contribution

The oxygen molecules whose proportion is constant in the atmosphere will also contribute a little due to their continuous spectrum in the frequency range of interest. The optical depths of oxygen at the two frequencies are slightly different, but $(T_1 - T_2)$ can be taken to be constant.

4.4.6.4 Liquid water

If there are clouds present in the beam of the radiometer, the water droplets in them will contribute to the observed antenna temperature. But their spectral characteristics are different from those of water vapour. Assuming their size to be small compared to the wavelength of the radiation under consideration, it is known that this contribution is proportional to ν^2 (Staelin, 1966), where ν is frequency of radiation. Therefore, f_1 contributes about 20% more than f_2 and there will be a residual effect due to this, if there are clouds at the time of observations. As a result, the observed $T_1 - T_2$ will be larger than the true value (due to vapour alone). For these reasons, the observations were restricted to conditions with no clouds or only light cloud cover.

4.5 Calibration of the radiometer

The radiometer output is $T_1 - T_2$ which should vary according to W. The values of $(T_1 - T_2)$ are plotted against computed W from simultaneous radiosonde ascents (Fig 4.15). A sufficiently large quantity of data was taken so as to get an average correlation between $T_1 - T_2$ and W.

The straight line indicates a linear least square fit, with a correlation coefficient of 0.76 upto 25 mm of W. The average rms difference between the fitted line and the observed values is about 3.5 mm, and somewhat more for higher W. A possible reason for this is the presence of clouds during those observations which gave the higher values. $(T_1 - T_2)$ includes side lobes and oxygen contribution, but they are not expected to affect the goodness of the fit because of their somewhat constant effect. A variation of the distribution of water vapour with height will affect when the same amount of water vapour (W) will give different values of $(T_1 - T_2)$ (Shimabukaro, 1966). For values of W lower than say 8 mm measured by the radiometer, the measurement error becomes appreciable compared to the measured value. Apart from these effects the uncertainty in the

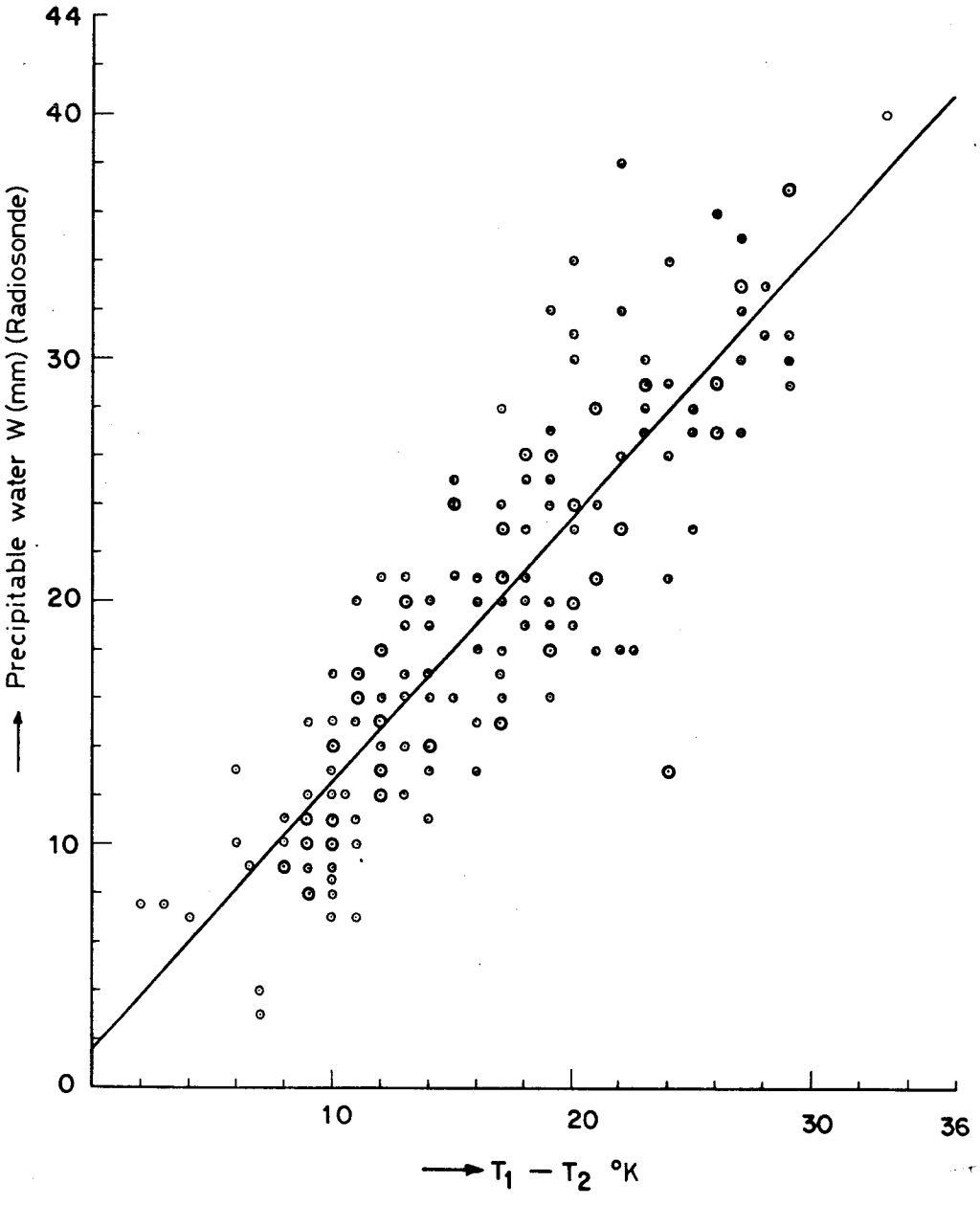

Fig. 4.15 Calibration curve of water vapour radiometer (showing W against T_1-T_2)

computed value of W from radiosonde data may also be a contributing factor. It was mentioned in Chapter 2 that the errors in the radiosonde measurements also increased at low values of W. It is therefore only in the range of 8 mm to 25 mm of W, that the agreement is reasonably good.

4.6 Computation of antenna temperature of MWR from radiosonde data

For comparison with the observed antenna temperature obtained with the radiometer, expected antenna temperatures were calculated from radiosonde (water vapour profile) data as follows:

The absorption coefficient α of water vapour in different atmospheric layers at different mean heights are calculated for the two frequencies 22.24 GHz and 20.5 GHz using the formula (4.7). This is possible since the temperature T, and the pressure p for each layer is known and d_v can be calculated using equation $d_v = \frac{217e}{T}$ for each layer, where e is partial pressure of water vapour in mb and T is the absolute temperature.

The total optical depth τ of the atmosphere due

to water vapour (corresponding to the two frequencies) can then be computed using the relation

$$\tau = \sum_{i=1}^{n} \alpha_i \Delta x_i \qquad (4.33)$$

where α_i and Δx_i are the absorption coefficient and thickness, respectively corresponding to the ith layer of the atmosphere, and n is the last layer of the atmosphere in the vertical direction for which humidity information is available.

Antenna temperatures can now be calculated using the following formula:

$$T_A = \sum_{i=1}^{n} T_i \left[1 - e^{-\alpha_i \Delta x_i}\right] \exp\left[-\sum_{j=1}^{i-1} \alpha_j \cdot \Delta x_j\right] \qquad (4.34)$$

T_1 and T_2, the antenna temperatures, at 22.24 GHz and 20.5 GHz, of a ground-based radiometer were calculated from the radiosonde data, using formula (4.34), for Bangalore, for the period October 1980 to

February 1981. The calculated values are compared with those observed. There is a linear relationship with the observed values being somewhat higher. The least square fit line is $(T_1 - T_2)_{calculated} = 0.81\ (T_1 - T_2)_{obs} - 0.86$. The correlation coefficient is 0.72 (RMS = 2.9). The higher observed values are partly due to side-lobe effects and a rough estimate indicates that the observed $(T_1 - T_2)$ is expected to be 12% larger due to this cause.

Using radiosonde data, the optical depths due water vapour τ_1 and τ_2 at the two working frequencies of the radiometer were calculated as explained above, using equation (4.33). They are found to be on the average 0.0063 neper and 0.0042 neper at 22.24 GHz and 20.5 GHz respectively per mm of W with a standard deviation of less than 5% of the mean. These are nearly equal to those reported by Ulich (1980) and Westwater (1980). Further, it was also found that $\frac{\tau_1}{\tau_2}$ remains almost constant and that its mean value is 1.52 with a standard deviation of about 0.07. All these computations were carried out for the set of radiosonde data mentioned earlier.

From the calculated value of antenna temperature

one can get the "mean radiating temperature" (T_o) (Westwater, 1978) for the atmosphere. It is given by

$$T_o = \frac{T_A}{1-e^{-\tau}} \tau \qquad (4.35)$$

Computations were carried out for a large number of radiosonde measurements. The average value of T_o corresponding to Bangalore was found to be 288 K $\pm$ 5K and was used in determining attenuations from the radiosonde data.

4.7 Estimation of optical depth of atmosphere due to water vapour

Employing the above value of T_o and assuming $\frac{\tau_1}{\tau_2}$ to be 1.52, τ_1 and τ_2 can be estimated as follows:

$$\tau_1 - \tau_2 = (\tau_1 - \tau_2)_{obs} - (\tau_1 - \tau_2)_{oxygen} \qquad (4.36)$$

$(\tau_1 - \tau_2)_{oxygen}$ is determined using the values given for 20.5 GHz and 30.1 GHz by Westwater (1980) and it is 0.00185 nep.

We have from equation (4.23),

$$(\tau_1 - \tau_2)_{obs} = \frac{T_1 - T_2}{1.12\,(288)} \qquad (4.37)$$

where $(T_1 - T_2)$ is the value observed with the radiometer, 1.12 is a term which approximately takes care of side-lobe effects and 288 is the value of T_o. $(T_1 - T_2)$ can be expressed in terms of W, from the following calibration equation.

$$W = 1.1\,(T_1 - T_2) + 1.6 \qquad (4.38)$$

Using equation (4.37) and (4.38) in (4.36), we get,

$$\tau_1 - \tau_2 = 0.0028W - 0.0064 \qquad (4.39)$$

where $(\tau_1 - \tau_2)$ is in nepers and W in mm of precipitable water.

Taking the value of $\frac{\tau_1}{\tau_2}$ as 1.52, equation 4.39 becomes,

$$0.52\,\tau_2 = 0.0028W - 0.0064$$

$$\tau_2 = 0.0054W - 0.0123$$

$$\tau_2 \text{ in dB} = 0.024W - 0.053, \text{ or}$$

$$\tau_2 \text{ in dB} = (T_1 - T_2)\,0.026 - 0.016 \qquad (4.40)$$

$$\tau_1 \text{ in dB} = 0.04\,(T_1 - T_2) - 0.024 \qquad (4.41)$$

It has been found that these calculated values are within 20% of those computed from radiosonde data for the range of W from 7 mm to 23 mm.

Thus, we have good evidence to support the view that the radiometer can be used with a fair degree of accuracy to obtain W, or to compute the optical depth due to water vapour at the working frequencies, in the range of W mentioned earlier.

4.8 Sources of error and accuracy of measurement

As discussed in Sec. 4.4.6, the measured value of $(T_1 - T_2)$ may be larger than that due to the water vapour content of atmosphere because of the side lobe and oxygen contributions and the effect of clouds, if present. The first two effects remain more or less constant and this systematic error will not affect the estimation of W because it is accounted for in calibration. But the presence of clouds will affect the measurement because the error introduced will vary with the liquid water content of the clouds and also on the size of the drops. Therefore, measurements are only reliable under cloudfree or light cloud conditions.

$(T_1 - T_2)$ will also depend upon the vertical distribution of water vapour apart from the total water

vapour content (Shimabukaro, 1966). This will lead to a small error in W. Night time observations may contain an additional small error, because of the few gain calibrations made at night.

Since the radiometer is switching between the two frequencies, the effect of gain variations due to temperature and supply voltage variations is minimised. Gain calibrations are done every two hours during day time and some times during night. Taking into consideration the errors in $(T_{R1} - T_{R2})$, the reading and setting errors, as mentioned in Sec. 4.4.6 an rms error of 10% is estimated for $T_1 - T_2$. However, for small values of $T_1 - T_2$, the error may be higher than the above estimated value. Similarly the error in the estimation of W may be also taken as 10% and may be higher for lower ($<$ 8mm) values of W.

Since at higher values W ($>$ 25mm) the scatter of points is greater, in the calibration graph, the values of W measured with the radiometer will have larger errors. In addition, any systematic error in radiosonde results are included in the estimated W, because radiosonde data formed the basis of calibration.

Therefore in the intermediate range of W (8mm to 25mm) the microwave water vapour radiometer can be said to give W an error of about 25%.

4.9 Measurements

From the millivoltmeter records obtained with the radiometer, the daily mean values of precipitable water were computed and are shown in Table 4.1 and Fig 4.16. A day is divided into 6 periods, 0600 - 1000, 1000 - 1400, 1400 - 1800, 1800 - 2200, 2200 - 0200 and 0200 - 0600 hours. Monthly means for each of these periods, and for the whole day were determined for the months September 1980 to April 1981 and are plotted in Fig 4.17. The results are discussed in Chapter 5.

4.10 Summary

A microwave water vapour radiometer designed and constructed by the author is described. The physical concepts, the nature of water vapour absorption in the microwave region and the relationship between the antenna temperature of the radiometer and the absorption coefficient of water vapour in the microwave region are described. From a discussion of the sources of error it is seen that the microwave radiometer can measure precipitable water in the range 8 to 25 mm with an accuracy of about 25 per cent.

Table 4.1: Mean daily values of precipitable water W over Bangalore determined by microwave water vapour radiometer

	January		February		March		April	
Date	1980	1981	1980	1981	1980	1981	1980	1981
1	9.5	14.3	8.8	-	18.3	13.2	32.1	26
2	11.9	16.4	17.8	14.9	26.8	12.3	31.4	28.9
3	16.6	17.7	13.5	13.9	19.5	12.2	26.8	26.6
4	13.4	9.7	17.4	12.6		10.4	24.3	27.1
5	11.3	8.7	20.2	19.8		9.7	23.8	28.9
6	16.8	11.5	13	19.1		10.3	-	24.9
7	13.5	10.8	13.8	20.9		13.4	32.1	24.1
8	12.5	11.1	7.7	17.8		15.5	26.8	21.9
9	12.9	15.7	6.4	19.3		14.8	24.6	16.6
10	11.3	17.8	8.2	18.2		20.0	27.8	13.9
11	8.7	17.1	11.2	18.4		25.1	32.1	16.2
12	10.7	18	10.5	19.4			29.4	16
13	7.5	17.2		17.8			23.8	16.2
14	9.5	16.5		20.8			23	22.8
15	10.4	19.7		-			28.1	28.4
16	11.1	30.7		13		21.0	24.8	32.7
17	11.1	-	14.3	-		22.2	31.7	26.2
18	8.1	21	12.2	8.6		27.2	37.3	29.9
19	10.6	19.9	13.4	10.8		25.4	35.3	
20	15.7	17.1	14.0		14.0	27.2		21.7
21	11.3	14.9	12.4		18.0	29.8	35	20.9
22	12	16.1	10.9	14.4	18.4		33.8	26.2
23	10.6	18.0	13.7	9.5		25.6	29.7	25.6
24	9.8	18.9	13.8	13	17	23	34.8	23.4
25	2.7	19.8	10.6	14.3	16.2	21.5	35.7	23
26	7.2	21.2	12.9	10.3	12.6	25.1	39.5	25.8
27	4.3	15.7	13.3	9.5	13.2	27.2		28.5
28	7.8	15.1	17.3	12.2	19.2	32.8	32.3	25.8
29	9.8	14.2			28.9	23.5	30.3	27.5
30	13.0	13.7				23.5	27.9	30.8
31	10.8	11.4			32.5	25.2		

....contd.

Table 4.1 contd.

Date	1980 May	June	July	Aug	Sep.	Oct.	Nov.	1979 December	1980
1	36.4	-		39	27.6		10.3	24	13.3
2	38.9	40		31.5	28.5		11.7	22	14.5
3		41.9		-	30		14.9	17.7	16.7
4		42.3		35.6	35.6		19.6	22.5	36.2
5		41.7		40	33		26.4	28.2	29.1
6		39.1		43.1	26.4	21.2	17.8	24.8	29.3
7	36.7	38.1		39.2	23.5	20.4	15.2	23.6	20.6
8	31.1	37.8			25.5	23.1	12.8	18.0	15.8
9	34.7	37.3			25.1	28.1	10.1	20.2	16.3
10	31.9	36.6			21.4	31.8	17.7	25.1	14.5
11		44.5			21.8	34.7	34	29.7	13.4
12		44.2			23.1			26.4	17.4
13	35.5	40.8			22.7	20.7		21.6	15.9
14	33.2	41			15.8	19.8		19.9	7.1
15	30.2	44			19.2	20.5		18.6	3.9
16	30.5	45.8	41		15.9	19.2		15.2	3.4
17	39	45.4	33.6		19.3	25.5		15.0	10.8
18	31.5	42.3	33.7		20.7	27.9		15.6	17.3
19	30.3		34		21.4	24.8		15.3	13.7
20	27.6		-		25.3	25.3		15.4	9.6
21	31.3		38.8			29.9	21.9	15.5	10.8
22	30.5		38			29.8	18.5	16.1	24.9
23	-		36.5			33.2	17.5	19.7	26.8
24	23.9		36.9			34.1	15.3	20.4	14.6
25	23.2		36.9			30.7	12.1	17.7	
26	28.1		35.6			25	12.4	15.7	
27	34.4		36.3	29.7		16.4	10.5	11.8	
28	37.4		37.8	23.1		14.5	7.8	9.3	
29	41.1		38.2	23.4		9.9	15.0	8.3	
30	36.4		38.4	30.1		11.8	23.6	8.0	12.8
31	46.4		38.3	34.2		11		8.3	13.6

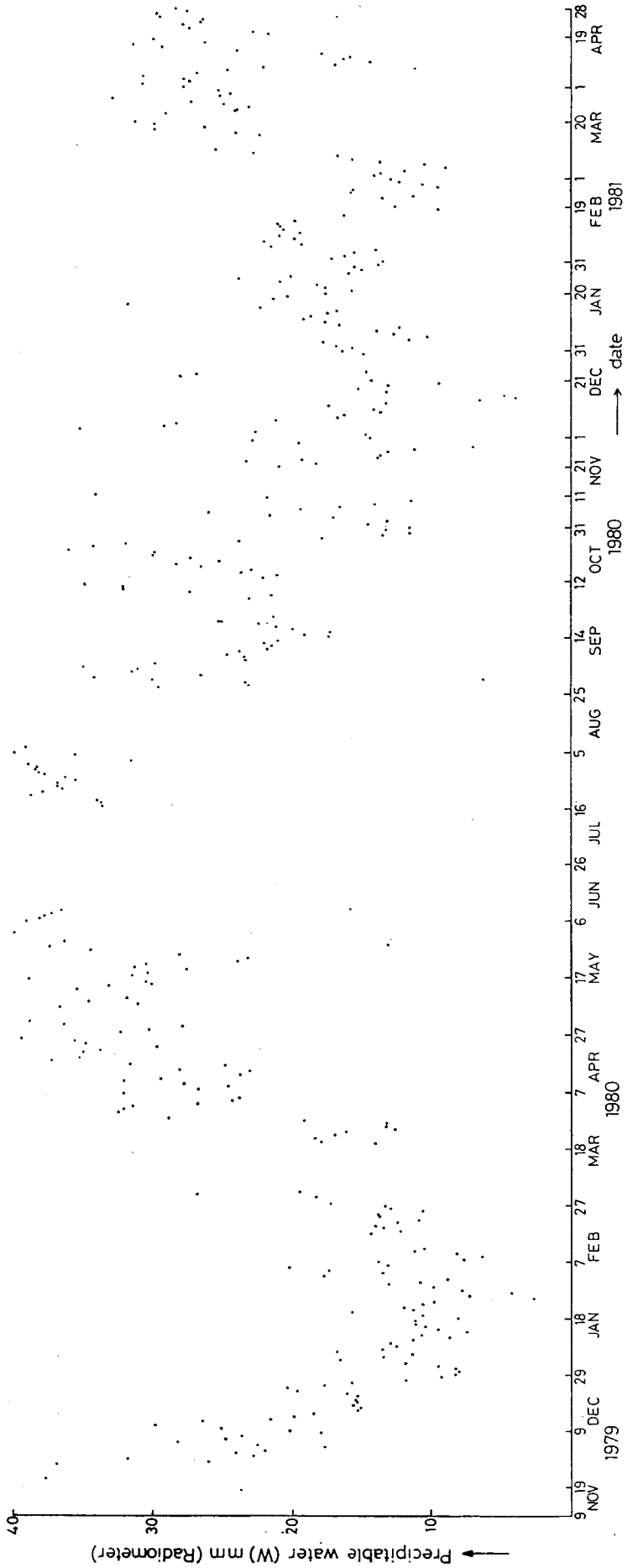

Fig. 4.16 Daily mean values of precipitable water vapour W over Bangalore measured with microwave water vapour radiometer.

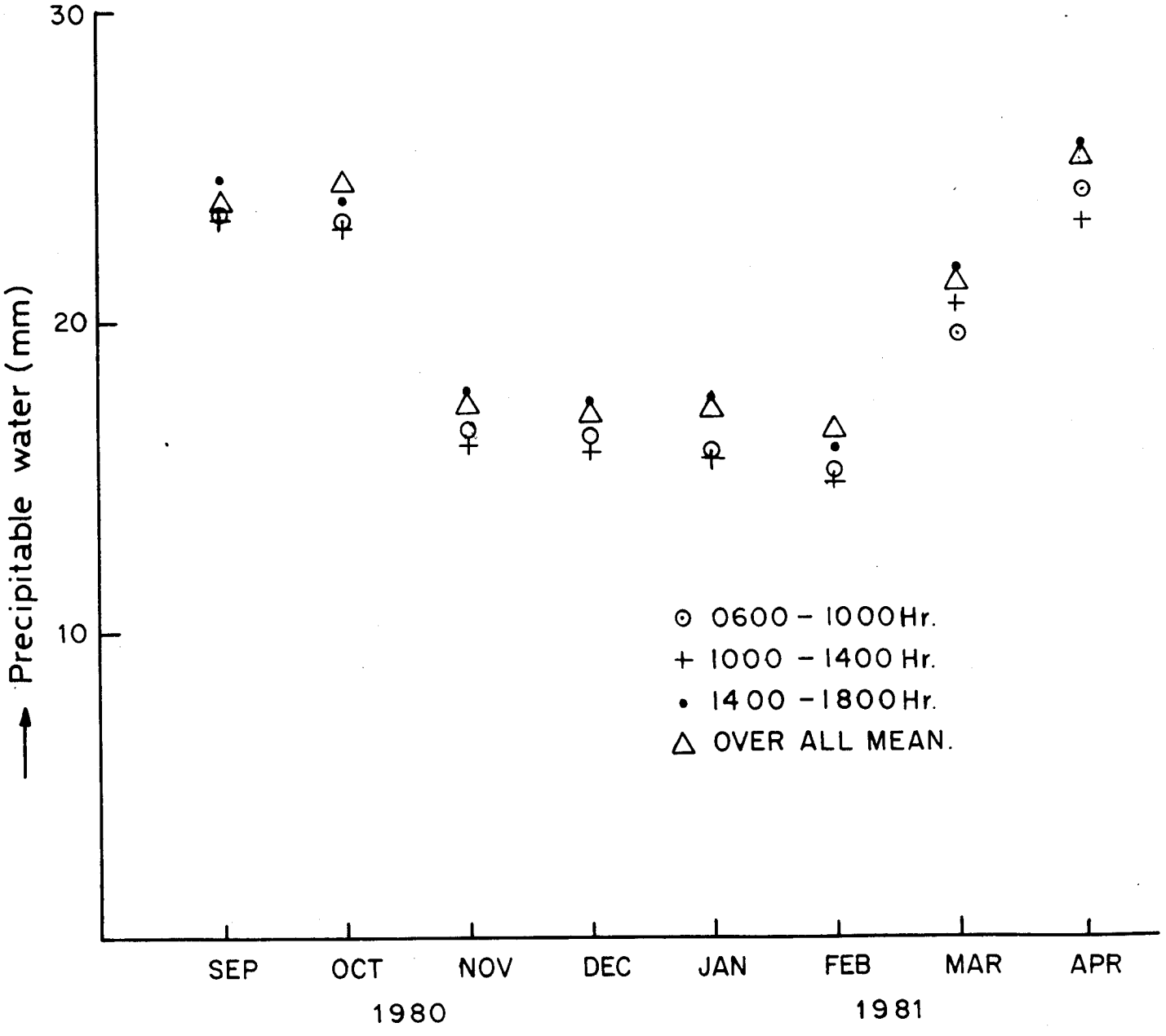

Fig 4.17: Monthly mean values of precipitable water W over Bangalore for various local hours

LIST OF FIGURES

LIST OF TABLES

REFERENCES

Barret. A.H., and Chung. V.K.	1962	A method for the determination of high altitude water vapour abundance from ground-based microwave observations, J. Geophys. Res., Vol. 67, No. 11, pp.4259-4266.
Dicke R.H.	1946	The measurement of thermal radiations at microwave frequencies, Review of Scientific Instruments, Vol. 17, No. 7, pp.268-275.
Dicke. R.H., Beringer. R., Kyhl. R.L. and Vane. A.B.	1946	Atmospheric absorption measurements with Microwave Radiometers, Physical Review, Vol. 70. No. 5 and 6, pp.340-348.
Gross. E.P.	1955	Shape of Collission-Broadened Spectral Lines Phys. Rev. Vol. 97, pp.395-403.
Guiraud. F.O. Howard J. and Hogg. D.C.	1979	A dual channel microwave radiometer for measurement of precipitable water vapour and liquid-IEEE Transaction on Geoscience Electronics, Vol. GE-17, No. 4, p. 129.
Kraus. J.D.	1966	Radio Astronomy, New.York, McGraw-Hill.

....contd.

Moore. R.K.	1975	Microwave Remote Sensors Chapter 9, Manual of Remote Sensing, Vol. I, American Society of Photogrammetry, Falls Church Va.
Penzias. A.A. and Burrus. C.A.	1973	Millimetre-wavelength radio-astronomy techniques, Ann. Rev. Astron. Astrophys, Vol. 11, pp. 51-71.
Rainwater. J.H.	1978	Radiometers: Electronic eyes that 'see' noise, Microwaves, Vol. 17, No. 9, pp. 58-62.
Shimabukaro. F.I.	1966	Propagation through the atmosphere at a wavelength of 3.3 mm, IEEE Transactions on Antennas and Propagation, Vol. AP-14, No. 2, pp. 228-235.
Staelin. D.H.	1966	Measurements and interpretation of the microwave spectrum of the terrestrial atmosphere near 1cm. wavelength, J. Geophys. Res., Vol. 71, No. 12, pp. 2875-2881.
Staelin.D.H.	1969	Passive Remote Sensing at Microwave wavelengths, Proceedings of IEEE, Vol. 57, No. 4, pp. 427-439.
Toong. H.D. and Staelin. D.H.	1970	Passive microwave spectrum measurements of atmospheric water vapour and clouds, J. Atmos. Sci., Vol. 27, pp. 781-784.
Ulich. B.L.	1980	Improved correction for millimetre-wavelength atmospheric attenuation, Astrophysical Letters, Vol. 21, pp. 21-28.

.....contd.

Waters. J.W.	1976	Absorption and emission by atmospheric gases in Methods of Experimental Physics, M.L. Meeks, Ed. Vol. 12, Part B, Academic Press, New York.
Westwater. E.R.	1978	The accuracy of vapour and cloud liquid determination by dual frequency ground based microwave radiometers, Radio Science, Vol. 13, No. 4, pp.677-685.
Van Vleck. J.H. and Weisskopf. V.F.	1945	On the shape of collision broadened lines, Rev. Mod. Phys., Vol. 17, pp. 227-236.